IEEE Access
Multidisciplinary | Rapid Review | Open Access Journal

Received September 8, 2020, accepted October 14, 2020, date of publication October 27, 2020, date of current version November 16, 2020.

Digital Object Identifier 10.1109/ACCESS.2020.3034187

The Effects of Manufacturing Parameters on Static Characteristics of Water Hydraulic Artificial Muscles

ZENGMENG ZHANG[1,2], YUNRUI JIA[1], JINKAI CHE[1], PEIPEI LIU[1], AND YONGJUN GONG[2,3]

[1]Naval Architecture and Ocean Engineering College, Dalian Maritime University, Dalian 116026, China
[2]Key Laboratory of Rescue and Salvage Engineering Liaoning Province, Dalian 116026, China
[3]International Joint Research Center for Subsea Engineering Technology and Equipment, Dalian Maritime University, Dalian 116026, China

Corresponding author: Yongjun Gong (dlmuwater@163.com)

This work was supported in part by the National Natural Science Foundation of China under Grant 51475064, in part by the National Key Research and Development Program under Grant 2017YFC0307003, in part by the Science and Technology Innovation Fund Project of Dalian under Grant 2019J12GX041, in part by the Fundamental Research Funds for the Central Universities of China under Grant 3132019351, and in part by the Natural Science Foundation of Liaoning Province under Grant 2020-HYLH-18.

ABSTRACT The static characteristics of water hydraulic artificial muscles (WHAMs) are related to operating parameters and manufacturing parameters. Operating parameters include working pressure and contraction ratio. Manufacturing parameters include initial braiding angle, fiber sleeve material, and initial rubber tube thickness. These manufacturing parameters fundamentally influence the static characteristics of artificial muscle. Orthogonal experiments were designed with an initial braiding angle of 25 degrees and 32 degrees, fiber sleeve of UHMWPE and aramid 1414, and initial rubber tube thickness of 2mm and 3mm to study the significance level of the effects of these factors and their interactions on the static characteristics of WHAMs. Experiments were carried out at different contractions to study the relationship between contraction force and working pressure, and Analysis of Variance (ANOVA) analyzed the test data. The analysis results showed that the significance level of the initial braid angle on WHAM's static characteristics is the most significant; the significance level of fiber sleeve material and initial rubber tube thickness on the static characteristics of WHAMs depends on the working pressure and contractions. The analysis results help people fabricate different WHAM types according to the working conditions, which help people better control the contraction forces.

INDEX TERMS Fiber sleeve material, initial braiding angle, rubber tube thickness, water hydraulic artificial muscles.

I. INTRODUCTION

Fluid/air-driven artificial muscles are new actuators, including pneumatic artificial muscles (PAMs), water hydraulic artificial muscles (WHAMs), and oil-hydraulic artificial muscles (OHAMs). Artificial muscle is a mechanical, pneumatic arm orthosis invented by Dr. Joseph L. McKibben in the 1950s to control the hands of the disabled [1]. This type of artificial muscle is called McKibben-type artificial muscle, mainly used for fingers' auxiliary treatment. PAM's typical structure can be regarded as a long bladder wrapped inside a fiber sleeve with a predetermined angle [2]. With reference to McKibben-type artificial muscle, a pneumatic bending actuator was designed by Tschiersky *et al.*, which is applied to assistive wearable robots [3].

PAMs have advantages such as low cost, simple installation, and good flexibility. PAMs are widely used in medical rehabilitation [4], industrial automation [5], robotics [6]–[8], and other fields [9], [10]. However, PAMs have low working pressure range and output force, limited transmission accuracy, and repeatability. PAM's working pressure and output forces are generally 0.2-0.8MPa and 100N-500N, respectively [10]–[13]. Compared with PAM, WHAM's working pressure is as high as 6MPa [14], the contraction force is as large as 28 kN [15]. Moreover, the air compressor's noise and vibration can be eliminated using a tap water drive [16].

The associate editor coordinating the review of this manuscript and approving it for publication was Jenny Mahoney.

Due to the significant difference in the working pressure and contraction force between PAMs and WHAMs, the fiber sleeve of WHAMs needs to bear more load, and the rubber tube needs to bear higher working pressure. Therefore, the higher strength of the fiber sleeve and larger thickness of the rubber tube are necessary. In some literature, the effects of initial braiding angle, fiber sleeve material, and rubber tube thickness on WHAM's static characteristics were studied through model optimization and experimental analysis. Nylon fiber, Kevlar fiber, aramid fiber, P-phenylene-2, 6-benzobisoxazole (PBO) fiber, and other fibers are generally used as the sleeve materials of artificial muscle [5], [15]–[17]. Mori *et al.* [15] compared the elasticity, fire resistance, and heat resistance of polyester, aramid, high-strength polyethylene (HS-PE) fibers, and PBO fibers. The PBO fiber with the best performance was selected to fabricate muscle. In the case of working pressure is 4 MPa, the maximum contraction force and contraction ratio of muscle were 28 kN and 25%, respectively. Furthermore, the experimental results suggested that artificial muscles' contraction ratio and contraction force increases with initial braiding angle declines. Kothera *et al.* [18] modified the existing mathematical model based on energy balance and force balance by considering the elastic force of a rubber tube and fiber sleeve's energy storage. Moreover, the improved model and the measured data shown that the improved model can predict muscle static response more accurately. Pillsbury *et al.* [19] fabricated and tested several PAMs with bladder thickness that varied between 0.397 mm and 0.794 mm. They verified that contraction force and free contraction both decrease with increasing bladder thickness. Thomalla and Van De Ven [20] developed a new variation of the Chou-Hannaford model to describe the relationship between contraction force, contraction ratio, and rubber tube thickness. The experimental results shown that the overall average error of the new model was 9.1%. Sangian *et al.* [21] found that the stiffnesses of natural latex with 0.28 mm and 0.56 mm thickness are 78 N/m and 150 N/m, respectively, and the experimental results of muscle shown that the stiffness of the inner tube have a considerable impact on artificial muscle performances.

In summary, artificial muscle's static characteristics are related to working pressure, contraction ratio, rubber tube thickness, fiber sleeve material, initial braiding angle, etc. Working pressure and contraction ratio of artificial muscles are operating parameters, which can be adjusted and optimized during the working process. The above research focuses on the effects of initial braiding angle, rubber tube thickness, and fiber sleeve material on the static characteristics of artificial muscle, while the significance level of these factors and their interactions on the static characteristics need to be further studied. Therefore, this research is dedicated to studying the significance level of the effect of these manufacturing parameters and their interaction on WHAMs. The main contribution of this work can be summarized as follows. This article reviews the artificial muscle models related to the initial braid angle, rubber tube thickness, and fiber sleeve's energy storage. Through experimental design and ANOVA, the significance level of the effects of manufacturing parameters on the static characteristics of WHAMs at different working conditions is obtained, which is suitable for facilitating the selection of manufacturing parameters to meet the required working conditions.

The rest of this paper is organized as follows. In Section 2, the structure, assembly, and working principle of WHAM are introduced, and theoretical analysis on manufacturing parameters is described. The WHAMs samples and experimental setup of the WHAM system are presented in Section 3. The experimental results and Analysis of Variance are carried out in Section 4. Finally, concluding remarks are given in Section 5.

II. THEORETICAL ANALYSIS OF STATIC CHARACTERISTICS OF WHAM

A. STRUCTURE AND WORKING PRINCIPLE OF WHAM

The structure and assembly of WHAM refer to Zhang *et al.*'s work [14]. A WHAM consists of a hollow end fitting, a closed-end fitting, crimping rings, a rubber tube, and a fiber sleeve, as shown in Figure 1. The fiber sleeve is longer than the rubber tube in the radial direction, as shown in Figure 1(A). A bamboo shoot shape and a shoulder exist on each of the two end fittings, namely, the close end fitting and the hollow end fitting, as shown in Figure 1(B) and (C). The assembly is shown in Figure 1(D)–(F). First, the two end fittings are plugged into the rubber tube at two ends, as shown in Figure 1(D). Second, the assemblage of the end fittings and the rubber tube is covered with the fiber sleeve, as shown in Figure 1(E). The sleeve is then clamped and pressed by a pair of crimping rings onto the two end fittings. During the working process, one end of the WHAM is closed, and the other end is connected to high-pressure water. With the increasing working pressure, the WHAM produces regular contraction and deformation under the fiber sleeve's restraint, generating corresponding contraction force and displacement. With the change in rubber tube thickness, fiber sleeve material, and initial braid angle, WHAM changes static characteristics. These factors affect the static characteristics of WHAMs in different degrees.

B. THE THEORETICAL ANALYSIS OF INFLUENCE OF MANUFACTURING PARAMETERS ON THE DRIVING CHARACTERISTICS OF ARTIFICIAL MUSCLES

Doumit *et al.* [22] and Chou and Hannaford [23] proposed an ideal model based on the principle of virtual work without considering the detailed geometric structure. The model assumes that the system is lossless and without energy storage, the extensibility of the shell thread is very low, and the ideal cylinder wall thickness is zero. However, in the manufacturing and practical application of muscle, the

bladder has a specific thickness, and the fiber is elastic [14], [15], [21]. Kothera *et al.* [18] and Thomalla and Van De Ven [20] developed a new model for the variation of bladder's thickness during the working process, and

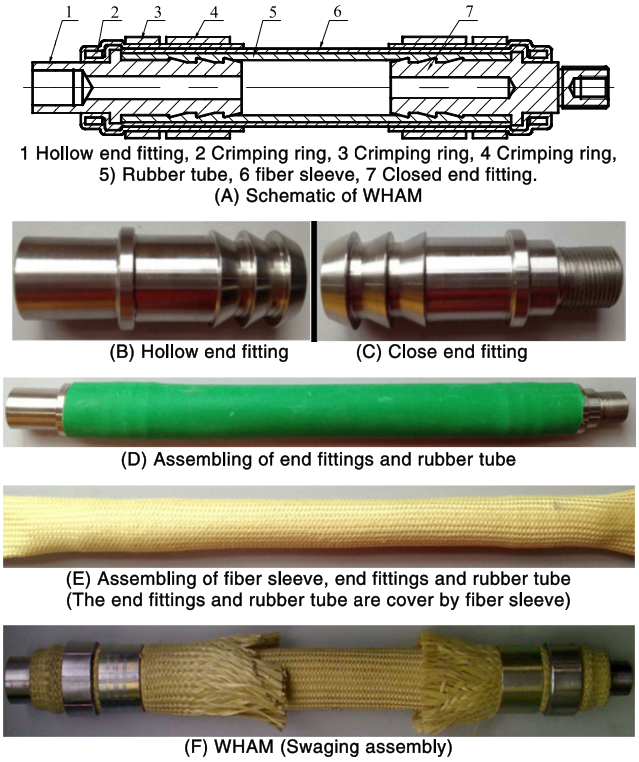

FIGURE 1. **The structure and assembly of WHAM.**

the overall average error between the new model and the experimental results was 9.1%. Zhefeng Yu *et al.* completed the hyperplastic analysis of PAM with the bladder. From the model analysis, the bladder's thickness significantly influences the free contraction of PAM. Furthermore, the experimental results show that the bladder's force was positive at small contractions and increased with the working pressure [24].

The theoretical contraction force expression of ideal cylindrical artificial muscle is

$$F_{\text{ideal}} = \frac{\pi D_0^2 p}{4}(3\cos^2\theta - 1) \tag{1}$$

where: F_{ideal}, p, D_0, and θ are contraction force, the working pressure, the initial outer diameter, and the current braiding angle, respectively. Tondu [25] derived the relationship of the current braiding angle θ and the initial braiding angle θ_0:

$$\frac{\cos\theta}{\cos\theta_0} = \frac{L}{L_0} = 1 - \frac{L_0 - L}{L_0} = 1 - \varepsilon \tag{2}$$

$$\frac{\sin\theta}{\sin\theta_0} = \frac{D}{D_0} \tag{3}$$

where: θ_0 is the initial braiding angle, L_0 is the initial effective expansion length, L is the current effective expansion length, ε is the contraction ratio, D is the current outside diameter. Combining formula (1), formula (2) and formula (3), the F_{ideal} is converted to

$$F_{\text{ideal}} = \frac{\pi D_0^2 p}{4}(3\cos^2\theta_0(1-\varepsilon)^2 - 1). \tag{4}$$

Refer to formula (4), contraction force F_{ideal} is related to operating parameters (working pressure p and contraction ratio ε) and manufacturing parameters (initial diameter D_0 and initial braiding angle θ_0). For given working pressure p, contraction ratio ε, and initial diameter D_0, the contraction force F_{ideal} of artificial muscle increases with the initial braiding angle θ_0 declining.

Kothera *et al.* [18] assumed that the volume of rubber tube is constant and the rubber tube produces an elastic force during the working process of the artificial muscle. The elastic force term for variable wall thickness is

$$F_{\text{elastic}} = E_r V_r\left(\frac{1}{L_0} - \frac{1}{L}\right) + \frac{E_r L}{2\pi r N^2}(tL - t_0 L_0) \tag{5}$$

$$r = \frac{r_0\sqrt{1-(1-\varepsilon)^2\cos^2\theta_0}}{\sin\theta_0} \tag{6}$$

$$t = r - \sqrt{r^2 - \frac{t_0(2r_0 - t_0)}{1-\varepsilon}} \tag{7}$$

where: E_r, V_r, r, N, t_0, t are the elastic modulus of rubber tube, the volume of rubber tube, the current outside diameter of rubber tube, the number of turns of single fiber about the rubber tube outside diameter, the initial wall thickness of elastic rubber tube and the current wall thickness of elastic rubber tube, respectively. Therefore, the expression of the axial contraction force of artificial muscle is

$$F_1 = F_{\text{ideal}} + E_r V_r\left(\frac{1}{L_0} - \frac{1}{L}\right) + \frac{E_r L}{2\pi r N^2}(tL - t_0 L_0) \tag{8}$$

Refer to formula (8), for given working pressure p, contraction ratio ε, initial diameter D_0, initial braiding angle θ_0, and fiber sleeve material, the contraction force of artificial muscle heightens with the wall thickness of rubber tube decreasing.

Kothera *et al.* [18] established the elasticity term on the fiber sleeve described as

$$F_{\text{braid}} = V_{\text{braid}}\frac{1}{E_{\text{braid}}A_{\text{braid}}^2 n^2}\frac{4\pi^2 p^2 B^2}{(2\pi N)^4}L \tag{9}$$

where: E_{braid}, V_{braid}, A_{braid}, n and B are the elastic modulus of the fiber, the total fiber sleeve volume, the cross-sectional area of single fiber, the number of fibers. Therefore, in the case of elastic energy storage in the fiber strand, the contraction force expression of the artificial muscle is

$$F_2 = F_{\text{ideal}} - V_{\text{braid}}\frac{1}{E_{\text{braid}}A_{\text{braid}}^2 n^2}\frac{4\pi^2 p^2 B^2}{(2\pi N)^4}L. \tag{10}$$

Refer to formula (10), the contraction force increases with the values of E_{braid} and A_{braid} increasing. To sum up, the initial braiding angle, rubber tube thickness, and fiber sleeve material are important manufacturing parameters that affect artificial muscles' static characteristics.

III. SAMPLE PREPARATION AND TEST SETUP

A. SAMPLE PREPARATION

To study the effect of initial braiding angle, fiber sleeve material, rubber tube thickness, and their interactions on the contraction forces of WHAMs, the samples and orthogonal

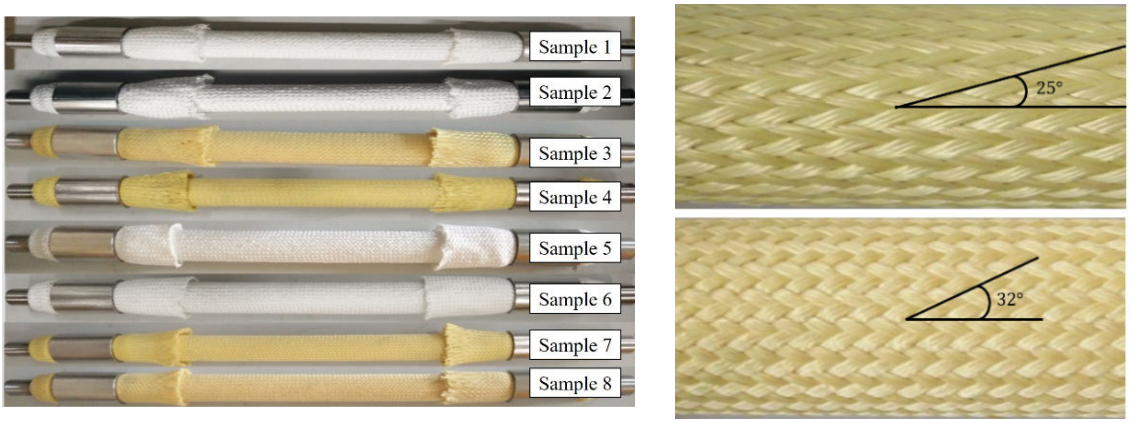

FIGURE 2. The samples of eight WHAMs.

TABLE 1. Test factors.

	1	2
A (Initial braiding angle /°)	25	32
B (Fiber sleeve material)	UHMWPE	Aramid1414
C (Rubber tube thickness /mm)	2	3

TABLE 2. The orthogonal of experiments.

Factor / Sample	A	B	A×B	C	A×C	B×C	blank
1	1	1	1	1	1	1	1
2	1	1	1	2	2	2	2
3	1	2	2	1	1	2	2
4	1	2	2	2	2	1	1
5	2	1	2	1	2	1	2
6	2	1	2	2	1	2	1
7	2	2	1	1	2	2	1
8	2	2	1	2	1	1	2

experiments on these factors were designed. Eight WHAMs were fabricated to analyze the effects of manufacturing parameters and their interaction on static characteristics. There are some commonalities among these actuators. First, the initial effective expansion length is 300 mm. Second, the rubber tube is made of neoprene, and the external diameter of the rubber tube is 30 mm. Third, the fiber sleeve is made of 96 spindles, and each spindle consists of three thin fiber bundles. Initial braiding angle, fiber sleeve material, and rubber tube thickness are defined as factor A, factor B, and factor C, respectively. The test factors are shown in Table 1. Factor A has two options: 25° and 32°. Factor B has two options: UHMWPE and Aramid1414. Factor C has two options: 2 mm and 3 mm. The orthogonal experiment $L_8(2^7)$ was arranged to search out the effects of these factors and their interaction on static characteristics, as shown in Table 2. The factor A×B is the interaction of factor A and factor B. The factor A×C is the interaction of factor A and factor C. The factor B×C is the interaction of factor B and factor C. The samples are shown in Figure 2, and the sample numbers in Table 2 correspond to the sample numbers in Figure 2.

B. TEST SETUP

The principle diagram of the static measurement system is shown in Figure 3. This static measurement system is used to measure the contraction force and working pressure of WHAMs at different contractions (L_0-L). The turnbuckle length was adjusted to control the contraction (L_0-L) of WHAMs, and the hydraulic half-bridge regulated the working pressure of WHAMs.

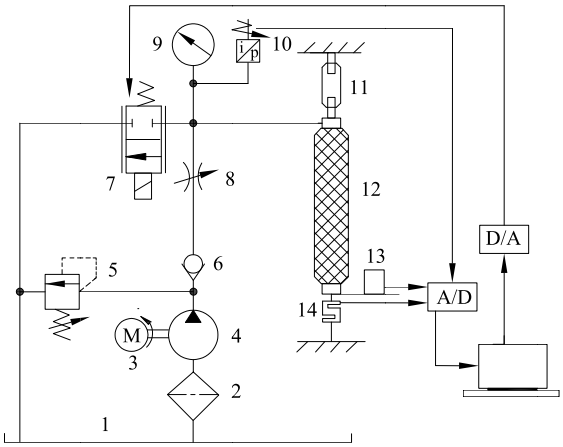

FIGURE 3. Principle diagram of static measurement system. 1 Water tank, 2 filter, 3 electric motor, 4 water hydraulic pump, 5 pressure relief valve, 6 check valve, 7 proportional throttle valve, 8 manual throttle, 9 pressure gauge, 10 pressure transmitter, 11 turn buckle, 12 WHAM, 13 wire-drawing displacement sensor, 14 tension sensor.

The test system is shown in Figure 4, which consists of 5 parts: power pack, data acquisition unit, pressure control unit, installation platform, and load system. The WHAM is mounted at the center of the installation platform. The hollow end fitting is connected to the upper mounting plate through a connector and tensioner, which is used to adjust the contraction of WHAMs. And closed-end fitting is connected

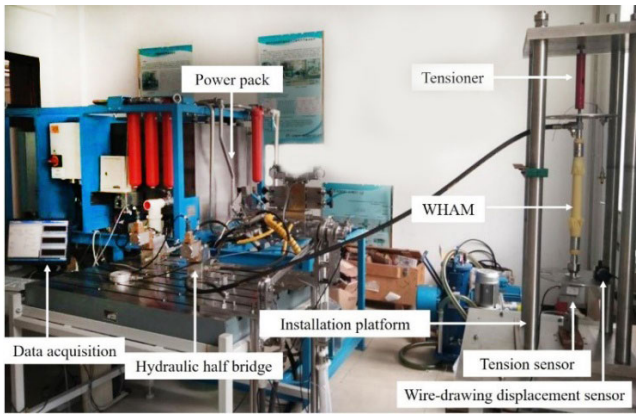

FIGURE 4. Test system of WHAM.

to the tension sensor, which is used to detect the contraction forces of WHAMs. The wire-drawing displacement sensor is mounted on the middle part to detect the contraction of the WHAMs. The power pack is a water hydraulic test platform manufactured by the Finnish HYTAR Company. The pressure control unit is a hydraulic half-bridge used to control the working pressure of WHAMs. A pressure sensor is connected to the water hydraulic proportional throttle valve to measure the working pressure of WHAMs.

The initial contraction was 0 mm, and the contraction ranges from 0 to 70 mm at a regular interval of 10mm during the test. The working pressure ranges from 0 to 4 MPa. The working pressure, contraction, and contraction force of WHAMs were collected by MATLAB®software. These sensors' performance indexes in the test system are shown in Table 3.

TABLE 3. Sensor parameters.

Sensor	Maximum range	Linearity	Output pressure
Wire-drawing displacement sensor	400 mm	0.1% FS	0-5 V
Pressure transmitter	10 MPa	0.1% FS	0-10 V
Tension sensor	30000 N	0.3% FS	0-10 V

IV. RESULTS AND DISCUSSIONS

A. ANALYSIS OF VARIANCE ON CONTRACTION

The curves describe the relationship between contraction ratio and working pressure of 8 WHAMs under no-load, as shown in Figure 5. The working pressure ranges from 0 to 4 MPa. The contraction ratio of 8 WHAMs at 4 MPa without load are shown in Table 4, and the Analysis of Variance is carried out. The F test is used to check the significance level of factors, and the critical value F_α (f_a, f_e) is determined according to the F table, where f_a is the degree of freedom of the sum of squares of factor a and f_e is the degree of freedom of the sum of squares of errors. Comparing each factor's critical value with F value, if F value > $F_{0.01}$ (f_a, f_e), this factor is highly significant; If $F_{0.01}$ (f_a, f_e) > F value > $F_{0.05}$ (f_a, f_e), this factor is significant; If $F_{0.05}$ (f_a, f_e) > F value > $F_{0.1}$ (f_a, f_e), it shows that this factor has influence; If $F_{0.1}$ (f_a, f_e) > F value > $F_{0.2}$ (f_a, f_e), it shows that this factor has some influence; If $F_{0.2}$ (f_a, f_e) > F value, it shows that this factor has no influence. In this variance analysis, $F_{0.01}$ (1,1) =4052, $F_{0.05}$ (1,1) = 161.4, $F_{0.1}$ (1,1) =39.86, $F_{0.2}$ (1,1) = 9.5. The analysis results are shown in Table 5. It can be observed that the initial braiding angle has the greatest influence on the contraction ratio of WHAM. With

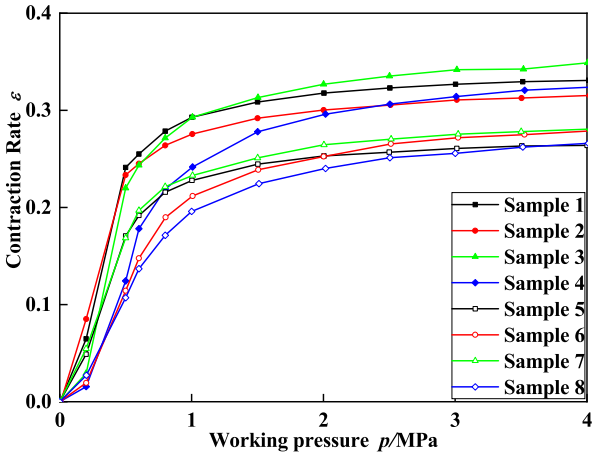

FIGURE 5. Relationship between contraction ratio and working pressure of 8 WHAMs.

TABLE 4. The contraction ratio of 8 WHAMs at 4 MPa without load.

Sample	Contraction ratio
1	0.331
2	0.315
3	0.349
4	0.324
5	0.264
6	0.279
7	0.281
8	0.266

TABLE 5. The analysis results of 8 WHAMs.

Factor	Sum of squares	DOF	F value	Significance level
A	6.56×10^{-3}	1	118.91	Influence
B	1.20×10^{-4}	1	2.18	No influence
A×B	6.61×10^{-5}	1	1.20	No influence
C	2.10×10^{-4}	1	3.81	No influence
A×C	2.10×10^{-4}	1	3.81	No influence
B×C	1.90×10^{-4}	1	3.45	No influence
Error	5.51×10^{-5}	1	-	-
Sum	7.41×10^{-5}	7	-	-

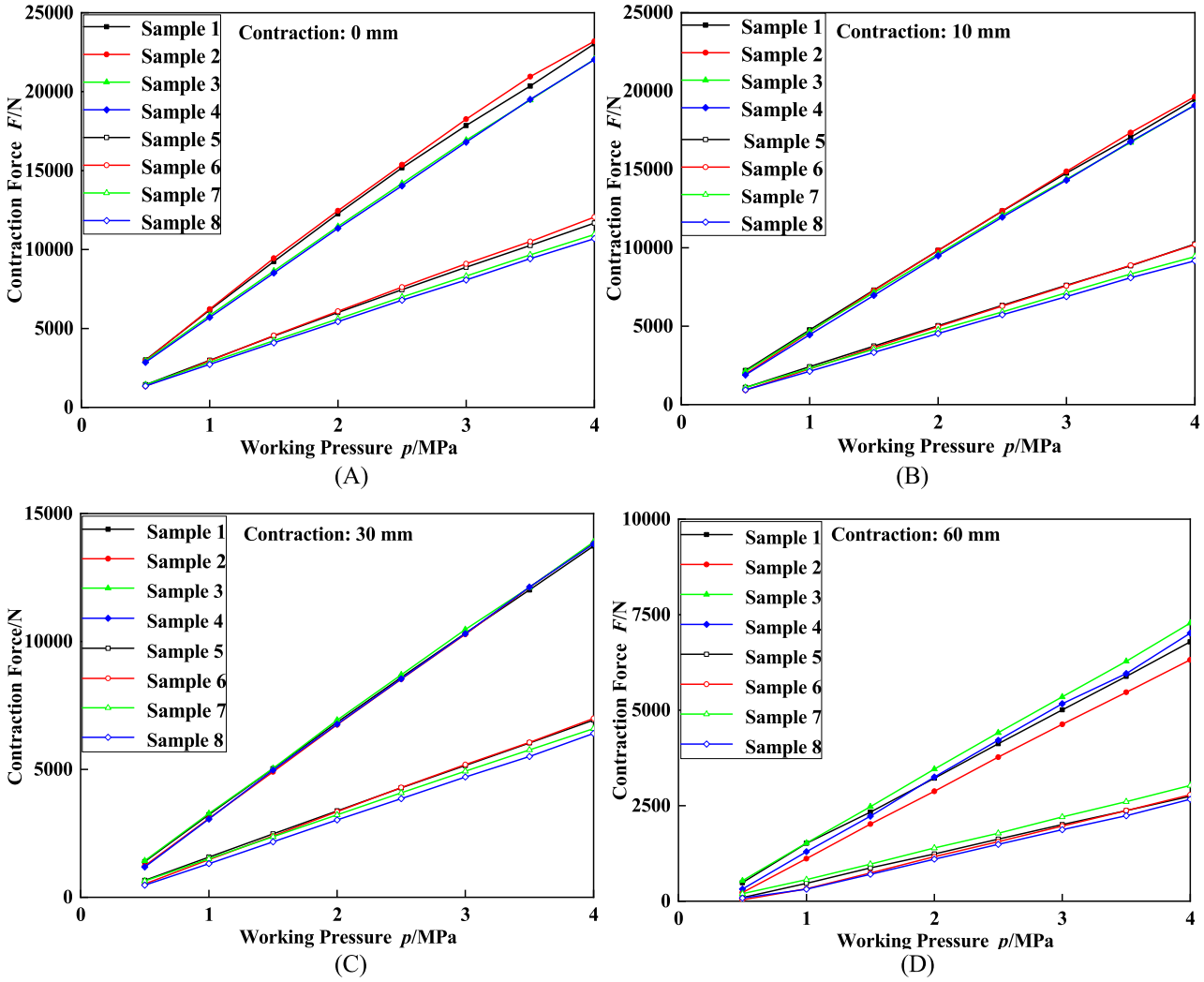

FIGURE 6. Relationship between contraction force and working pressure.

TABLE 6. Contraction force of WHAMs at 30 mm contraction.

Force/N / Sample	0.5MPa	1MPa	2MPa	4MPa
1	1394.330	3231.978	6842.128	13736.133
2	1229.636	3081.326	6747.070	13860.869
3	1429.362	3276.774	6932.804	13893.198
4	1182.292	3059.106	6765.401	13819.406
5	660.553	1572.428	3376.694	6926.082
6	518.109	1468.006	3345.894	6993.321
7	634.527	1505.127	3222.046	6593.628
8	471.632	1315.030	3022.239	6405.695

the influence of factor A, factor B has less influence on the contraction ratio than factor C.

B. ANALYSIS OF VARIANCE ON CONTRACTION FORCE

The static test in the contraction of 0 mm, 10 mm, 20 mm, 30mm, 40 mm, 50 mm, 60 mm, and 70 mm was carried out. Furthermore, the relationships between working pressure and contraction force in 0 mm, 10 mm, 30 mm, and 60 mm are shown in Figure 6. It can be observed that the initial braiding angle plays a crucial role in the contraction force. The contraction forces of WHAMs at working pressures of 0.5 MPa, 1 MPa, 2 MPa, and 4 MPa in the case of 30 mm contraction are shown in Table 6. The F test's significance level is examined, and the analysis results are shown in Table 7. With the increase of working pressure, the influence of the factor B and the interaction of factor A and factor B on the contraction forces of WHAMs increase, and the influence of factor C on the contraction forces of WHAMs decline. The interaction of factor B and factor C and the interaction of factor A and factor C have almost no effect on the contraction forces of WHAMs. The F test analyzes each factor's significance level in the case of contraction of 0 mm, 10 mm, 20 mm, 40 mm, 50 mm, 60 mm, and 70 mm in the same way. The analysis results show that each factor's significance level in the case of contraction between 0 mm and 20 mm is the same as that in the case of 30 mm contraction. The analysis results

TABLE 7. Analysis of variance at different pressures with contraction of 30 mm.

Working pressure		A	B	A×B	C	A×C	B×C
0.5MPa	F value	2270.64	1.88	0.94	134.10	2.95	2.76
	Significance level	significant	no influence	no influence	influence	no influence	no influence
1MPa	F value	132374.45	112.27	169.41	1262.00	15.65	66.97
	Significance level	highly significant	influence	significant	significant	Some influence	influence
2MPa	F value	21948.57	14.60	36.92	26.02	0.11	6.23
	Significance level	highly significant	Some influence	Some influence	Some influence	no influence	no influence
4MPa	F value	251216.19	201.71	334.30	1.52	9.18	64.15
	Significance level	highly significant	significant	significant	no influence	no influence	influence

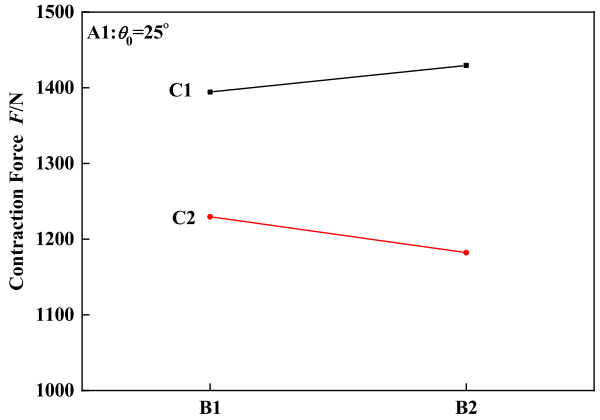

FIGURE 7. Relationship between contraction force and working pressure.

in the case of the contraction between 40 mm and 70 mm are as follows. Factor A has the most significant influence on the contraction force of WHAMs. With working pressure increases, the influence of factor C on the contraction force of WHAMs decreases. Factor B, the interaction of factor A and factor B, the interaction of factor B and factor C, and the interaction of factor A and factor C have little effect on contraction forces of WHAMs.

From Figure 6, the initial braiding angle plays a decisive role in the contraction force of WHAMs. The contraction force of WHAMs in the case of 25 degrees initial braiding angle is much larger than that in the case of 32 degrees initial braiding angle. According to the orthogonal test, WHAM's manufacturing parameters reach the maximum contraction force are determined as the optimal level. To analyze the optimal level of contraction force of WHAMs under different contractions and working pressures, a binary diagram of factor B and factor C was plotted with an initial braiding angle of 25 degrees. The binary diagram of WHAMs in the contraction of 30 mm and working pressure of 0.5 MPa is shown in Figure 7. The result shows that the optimal level of contraction force is A1 B2 C1, that is, the initial braid angle is 25 degrees, the fiber sleeve material is Aramid 1414, and the initial thickness of the rubber tube is 2 mm. When the contraction is 30 mm, the contraction force's optimal level is constant at different working pressures. The optimal level of contraction force's analysis results at different working pressures and contractions are as follows. When the contraction is 0mm to 20 mm, the optimal level of contraction force is A1 B1 C1, namely, the initial braiding angle is 25 degrees, the fiber sleeve material is UHMWPE fiber, and the initial rubber tube thickness is 2 mm; When the contraction is 30 mm to 70 mm, the optimal level of contraction force is A1 B2 C1, namely, the initial braiding angle is 25 degrees, the fiber sleeve material is Aramid 1414 fiber, and the initial rubber tube thickness is 2 mm.

C. RUBBER TUBE THICKNESS AND FIBER SLEEVE

Sample 1, sample 2, sample 3, and sample 4 are selected to analyze the effect of single factor B and factor C on contraction force. The effect of the rubber tube thickness on the contraction force is shown in Figure 8. Figure 8 (A) shows that when the contraction is in the range of 0 mm to 40 mm, the difference of contraction force of sample 1 and sample 2 does not exceed 0.88%. When the contraction is 40mm, sample 1 and sample 2 have the same contraction force, i.e. point A. When the contraction is in the range of 40 mm to 70 mm, the difference of contraction force between sample 1 and sample 2 increases with the contraction. From Figure 8 (B), when the contraction is in the range of 0 mm to 40 mm, the difference of contraction force of sample 3 and sample 4 does not exceed 1.1%. When the contraction is 40mm, sample 1 and sample 2 have the same contraction force, i.e. point B. When the contraction is in the range of 40 mm to 70 mm, the difference of contraction force between sample 1 and sample 2 increases with the contraction. The results suggest that with the increase of WHAM's contraction, the rubber tube thickness's influence on contraction force increases.

Hardness is a usual way to characterize elastomers, and it is often used as a rough correlation to a Young's hardness

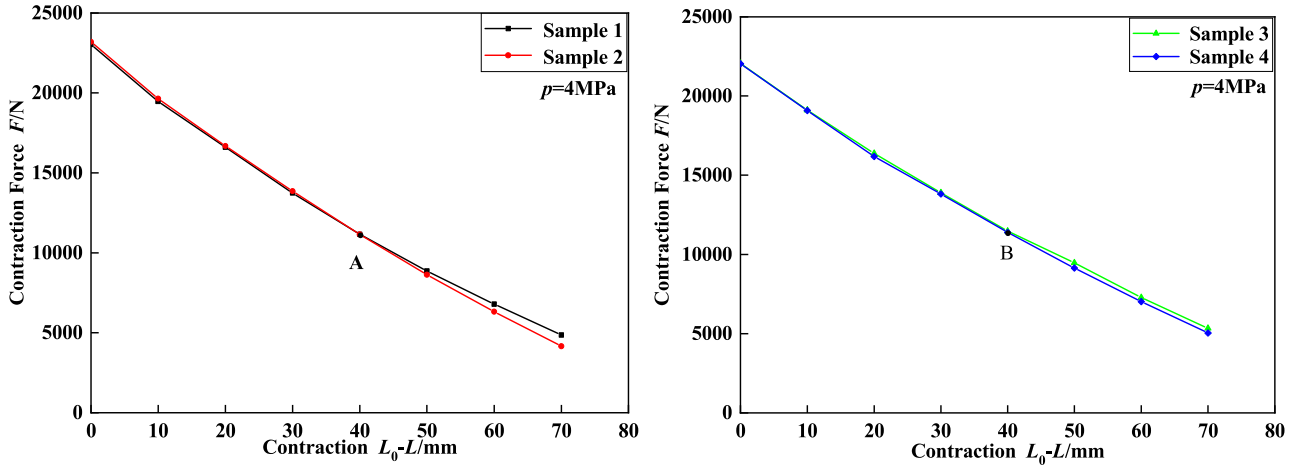

(A) Fiber sleeve material is UHMWPE (B) Fiber sleeve material is Aramid1414

FIGURE 8. Effect of rubber tube thickness on contraction force of WHAMs.

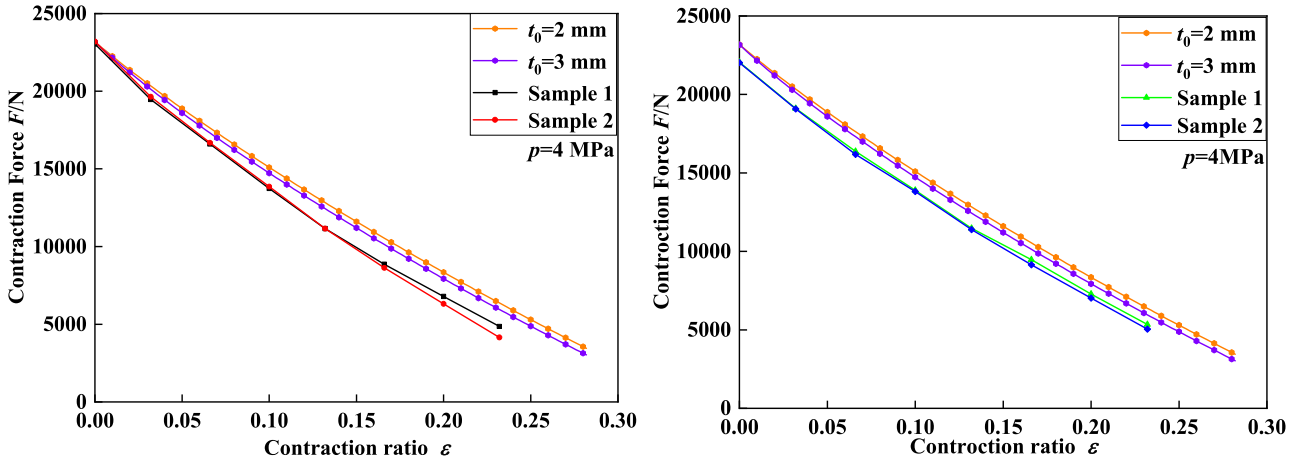

(A) Fiber sleeve material is UHMWPE (B) Fiber sleeve material is Aramid1414

FIGURE 9. Comparison between theoretical curve and experimental results.

of rubber materials to the Young's modulus [26]. The Gent model [20] is presented as

$$E = \frac{0.0981(56 + 7.62336S)}{0.137505(254 - 2.54S)} \tag{11}$$

where: E is the Young's modulus in megapascal and S is the durometer of the elastomer. The rubber tube was cut into test samples, which was about 65mm long and 40 mm wide. LX-A type durometer was used to measure the hardness of the rubber tube. The rubber tube samples' hardness was measured at an interval of 6 mm along the axial direction, and the results were shown in Table 8. Combining with the formula (5)-(8) and formula (11), the theoretical curves affected by the rubber tube thickness and the experimental results are shown in Figure 9. Figure 9 shows that the influence of initial rubber tube thickness will increase with the contraction ratio and the trend of the experimental results is consistent with the theoretical curve. The fiber sleeve's energy storage may cause the difference between the theoretical and experimental results.

TABLE 8. Hardness of rubber tube samples.

Number / Sample	1	2	3	4	5	6	Average value
t_0=2 mm	67	69	71	70	68	70	69.167
t_0=3 mm	71	69	69	71	70	71	70.167

The effect of the fiber sleeve material on contraction force is shown in Figure 10. Figure 10 (A) shows that sample 1 and sample 3 have the same contraction force at point C, whose contraction is defined as L_C. When the contraction does not exceed L_C, the contraction force of sample 1 is bigger than that of sample 3. When the contraction exceeds L_C, the contraction force of sample 1 is smaller than that of sample 3. Figure 10 (B) shows that sample 1 and sample 3 have the same contraction force at point D, whose contraction is defined as L_D. When the contraction does not exceed L_D, the contraction force of sample 2 is bigger than that of sample 4. When the contraction exceeds L_D, the contraction force of sample 2 is

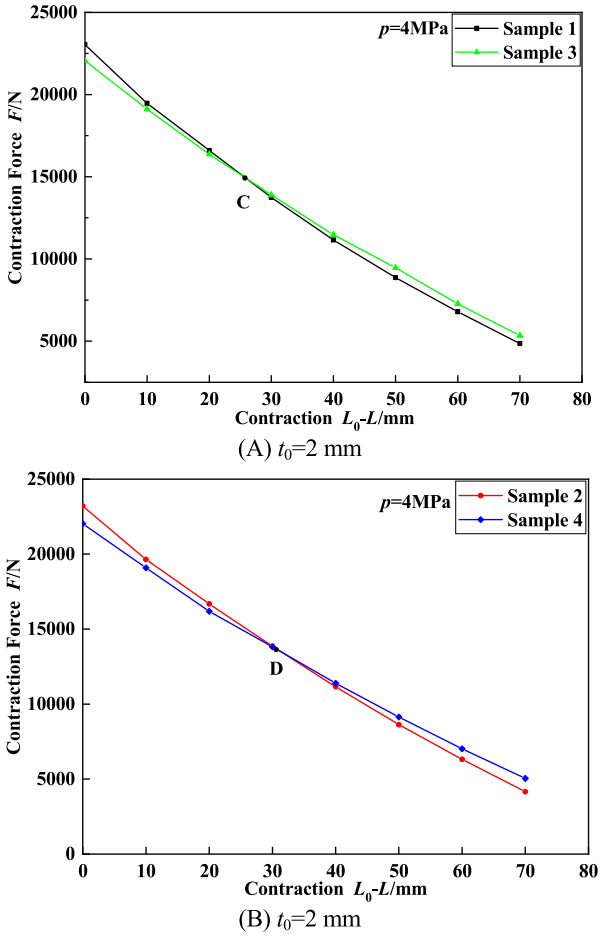

FIGURE 10. Effect of the fiber sleeve material on contraction force of WHAMs.

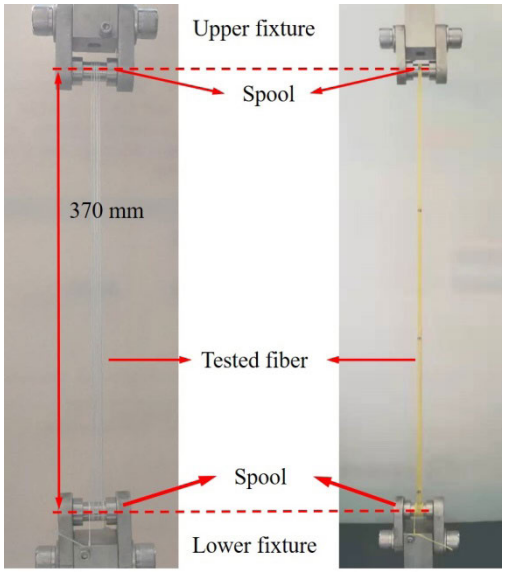

FIGURE 11. Fiber testing device.

less than that of sample 4. Two kinds of fibers were tested for tensile characteristics. The fiber tensile performance was tested by using a CTM8010 microcomputer-controlled

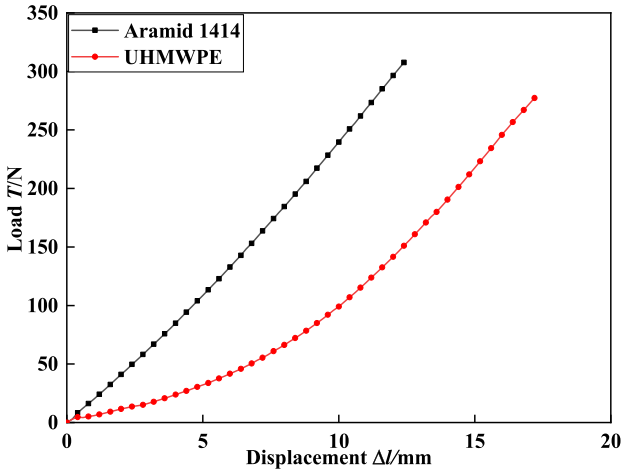

FIGURE 12. Fiber tensile characteristic.

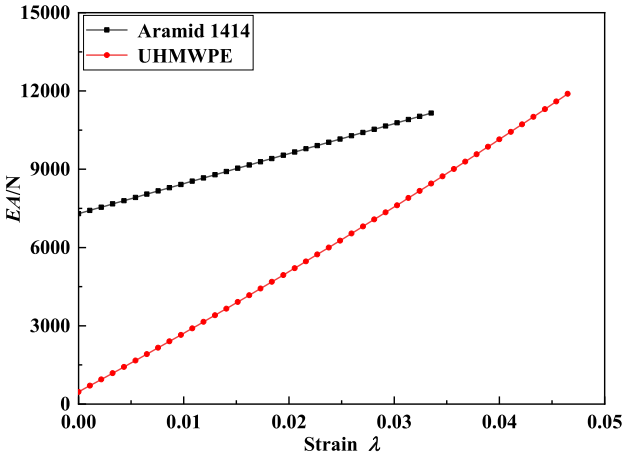

FIGURE 13. The relationship between EA and λ.

electronic universal material testing machine, which has a maximum load of 10 kN and the maximum error of less than 0.01%. The fibers were formed by winding a single fiber in parallel between two spools to ensure uniform force on the fiber and no friction between the fibers, as shown in Figure 11. The distance between the center axes of the spools was 370 mm. In the test, the number of turns of the tested fiber around the spools was 10. The relationship between load and displacement is shown in Figure 12. The elastic modulus E of fiber is defined as

$$E = \frac{\sigma}{\lambda} = \frac{T}{A} \Big/ \frac{\Delta l}{l} \tag{12}$$

where: σ, λ, T, A, Δl and l are the stress of fiber, the strain of fiber, the load of fiber, the cross-sectional area of fiber, the displacement of fiber and the initial length of fiber, respectively.

The relationship between the strain λ of fiber, the product of the elastic modulus E and the cross-sectional area of fiber A and the strain λ of fiber is

$$EA = \frac{T}{\lambda}. \tag{13}$$

From formula (9) and formula (10), WHAM's contraction force is related to the product of the elastic modulus E and cross-sectional area of fiber A. The relationship between the strain λ, the product of the elastic modulus E, and the cross-sectional area of fiber A is shown in Figure 13. Refer to formula (10), Figure 10, Figure 12, and Figure 13, it can be found that when the contraction does not exceed L_C, sample 1's product of E and A is bigger than sample 3. When the contraction exceeds L_C, sample 1's E and A products are smaller than sample 3. When the contraction does not exceed L_D, sample 2's E and A products are bigger than sample 4. When the contraction exceeds L_D, sample 2's E and A products are bigger than sample 4.

V. CONCLUSION

In this paper, the initial braiding angle, the fiber sleeve material, and the rubber tube thickness are regarded to affect the static characteristics of WHAMs through theoretical analysis. To study the influence of these factors and their interactions on the static characteristics of WHAMs, tests of the relationship between contraction force and working pressure at different contractions were carried out, and the data was analyzed. The conclusions are as follows.

The initial braiding angle has the most significant effect on the contraction force and contraction ratio of WHAMs. At the same other conditions, the contraction force of WHAMs increases with the initial braiding angle and the rubber tube thickness of declining.

When the other manufacturing parameters and working pressure are the same, WHAMs with different fiber sleeve materials have the same contraction force at a specific contraction. When WHAM's contraction is lower than the specific contraction, the UHMWPE's product of elastic modulus E and the cross-sectional area of fiber A is bigger than that of Aramid 1414. When WHAM's contraction exceeds the specific contraction, the UHMWPE's product of elastic modulus E and the cross-sectional area of fiber A is smaller than that of Aramid 1414.

The factors' significance levels are as follows. The interaction of initial braiding angle and rubber tube thickness and fiber material interaction and rubber tube thickness are no influence. The initial braiding angle has the greatest influence on the contraction force of WHAMs. In the case of the contraction is in the range from 0 to 30 mm, the fiber sleeve material is highly significant; the interaction of initial braiding angle and fiber material is significant; the rubber tube thickness is significant. In the case of the contraction is in the range from 40 to 70 mm, the fiber sleeve material, the interaction of initial braiding angle and fiber material are no influence. And the rubber tube thickness has some influence on the contraction force of WHAMs.

REFERENCES

[1] J. Sarosi, I. Biro, J. Nemeth, and L. Cveticanin, "Dynamic modeling of a pneumatic muscle actuator with two-direction motion," *Mechanism Mach. Theory*, vol. 85, pp. 25–34, Mar. 2015.
[2] S. Davis and D. G. Caldwell, "Braid effects on contractile range and friction modeling in pneumatic muscle actuators," *Int. J. Robot. Res.*, vol. 25, no. 4, pp. 359–369, Apr. 2006.
[3] M. Tschiersky, E. E. G. Hekman, D. M. Brouwer, J. L. Herder, and K. Suzumori, "A compact McKibben muscle based bending actuator for Close-to-Body application in assistive wearable robots," *IEEE Robot. Autom. Lett.*, vol. 5, no. 2, pp. 3042–3049, Apr. 2020.
[4] T. Noritsugu and T. Tanaka, "Application of rubber artificial muscle manipulator as a rehabilitation robot," *IEEE/ASME Trans. Mechatronics*, vol. 2, no. 4, pp. 259–267, Dec. 1997.
[5] D. G. Caldwell, N. Tsagarakis, G. A. Medrano-Cerda, J. Schofield, and S. Brown, "A pneumatic muscle actuator driven manipulator for nuclear waste retrieval," *Control Eng. Pract.*, vol. 9, no. 1, pp. 23–36, Jan. 2001.
[6] S. Xie, G. Ren, J. Xiong, and Y. Lu, "A trajectory tracking control of a robot actuated with pneumatic artificial muscles based on hysteresis compensation," *IEEE Access*, vol. 8, pp. 80964–80977, 2020.
[7] P. Beyl, K. Knaepen, S. Duerinck, M. Van Damme, B. Vanderborght, R. Meeusen, and D. Lefeber, "Safe and compliant guidance by a powered knee exoskeleton for robot-assisted rehabilitation of gait," *Adv. Robot.*, vol. 25, no. 5, pp. 513–535, Jan. 2011.
[8] T. Tagami, T. Miyazaki, T. Kawase, T. Kanno, and K. Kawashima, "Pressure control of a pneumatic artificial muscle including pneumatic circuit model," *IEEE Access*, vol. 8, pp. 60526–60538, 2020.
[9] J. Zhong and C. Zhao, "A phenomenological model-based controller for position tracking of a pneumatic muscle actuator driven setup," *IEEE Access*, vol. 7, pp. 45662–45669, 2019.
[10] Z. Zhang and M. Philen, "Pressurized artificial muscles," *J. Intell. Mater. Syst. Struct.*, vol. 23, no. 3, pp. 255–268, Feb. 2012.
[11] D. G. Caldwell, G. A. Medrano-Cerda, and M. Goodwin, "Control of pneumatic muscle actuators," *IEEE Control Syst. Mag.*, vol. 15, no. 1, pp. 40–48, Feb. 1995.
[12] R. M. Robinson, C. S. Kothera, and N. M. Wereley, "Quasi-static nonlinear response of pneumatic artificial muscles for both agonistic and antagonistic actuation modes," *J. Intell. Mater. Syst. Struct.*, vol. 26, no. 7, pp. 796–809, May 2015.
[13] E. G. Hocking and N. M. Wereley, "Analysis of nonlinear elastic behavior in miniature pneumatic artificial muscles," *Smart Mater. Struct.*, vol. 22, no. 1, Jan. 2013, Art. no. 014016.
[14] Z. Zhang, J. Hou, D. Ning, X. Gong, and Y. Gong, "Modeling and experiments on the drive characteristics of high-strength water hydraulic artificial muscles," *Smart Mater. Struct.*, vol. 26, no. 5, May 2017, Art. no. 055023.
[15] M. Mori, K. Suzumori, S. Seita, M. Takahashi, T. Hosoya, and K. Kusumoto, "Development of very high force hydraulic McKibben artificial muscle and its application to shape-adaptable power hand," in *Proc. IEEE Int. Conf. Robot. Biomimetics (ROBIO)*, Dec. 2009, pp. 1457–1462.
[16] W. Kobayashi and K. Ito, "Displacement estimation of tap-water driven McKibben muscles," in *Proc. Int. Conf. Fluid Power Mechatronics (FPM)*, Aug. 2015, pp. 672–676.
[17] T. Nakamura, N. Saga, and K. Yaegashi, "Development of a pneumatic artificial muscle based on biomechanical characteristics," in *Proc. IEEE Int. Conf. Ind. Technol.*, Dec. 2003, pp. 729–734.
[18] C. S. Kothera, M. Jangid, J. Sirohi, and N. M. Wereley, "Experimental characterization and static modeling of McKibben actuators," *J. Mech. Des.*, vol. 131, no. 9, Sep. 2009, Art. no. 091010.
[19] T. E. Pillsbury, C. S. Kothera, and N. M. Wereley, "Effect of bladder wall thickness on miniature pneumatic artificial muscle performance," *Bioinspiration Biomimetics*, vol. 10, no. 5, Sep. 2015, Art. no. 055006.
[20] S. D. Thomalla and J. D. Van De Ven, "Modeling and implementation of the McKibben actuator in hydraulic systems," *IEEE Trans. Robot.*, vol. 34, no. 6, pp. 1593–1602, Dec. 2018.
[21] D. Sangian, S. Naficy, G. M. Spinks, and B. Tondu, "The effect of geometry and material properties on the performance of a small hydraulic McKibben muscle system," *Sens. Actuators A, Phys.*, vol. 234, pp. 150–157, Oct. 2015.
[22] M. Doumit, A. Fahim, and M. Munro, "Analytical modeling and experimental validation of the braided pneumatic muscle," *IEEE Trans. Robot.*, vol. 25, no. 6, pp. 1282–1291, Dec. 2009.
[23] C.-P. Chou and B. Hannaford, "Measurement and modeling of McKibben pneumatic artificial muscles," *IEEE Trans. Robot. Autom.*, vol. 12, no. 1, pp. 90–102, Feb. 1996.
[24] Z. Yu, T. Pillsbury, G. Wang, and N. M. Wereley, "Hyperelastic analysis of pneumatic artificial muscle with filament-wound sleeve and coated outer layer," *Smart Mater. Struct.*, vol. 28, no. 10, Oct. 2019, Art. no. 105019.

[25] B. Tondu, "Modelling of the McKibben artificial muscle: A review," *J. Intell. Mater. Syst. Struct.*, vol. 23, no. 3, pp. 225–253, Feb. 2012.
[26] A. N. Gent, "On the relation between indentation hardness and Young's modulus," *Rubber Chem. Technol.*, vol. 31, no. 4, pp. 896–906, Sep. 1958.

ZENGMENG ZHANG was born in Jinan, China, in 1979. He received the Ph.D. degree in mechanical and electronics engineering from Zhejiang University, China, in 2009. He is currently a Professor and Doctoral Supervisor with the Naval Architecture and Ocean Engineering College, Dalian Maritime University, Dalian, China. He has published more than 30 articles in important academic journals and international conferences at home and abroad, of which more than 20 articles have been retrieved by SCI and EI. His current research interests include underwater intelligent electromechanical hydraulic equipment, and water hydraulic components and systems. He focused on the high-strength water hydraulic artificial muscle and its joint driving technology, high-performance hydraulic control valve, and other basic research work.

YUNRUI JIA was born in Tianjin, China, in 1996. He received the bachelor's degree in rescue and salvage engineering from Dalian Maritime University in 2014, where he is currently pursuing the master's degree in rescue and salvage engineering. His research interests include high-strength water hydraulic artificial muscles and bionic robots.

JINKAI CHE was born in Yulin, China, in 1995. He received the bachelor's degree in rescue and salvage engineering from Dalian Maritime University, Dalian, China, in 2013, where he is currently pursuing the Ph.D. degree in rescue and salvage engineering. His research interests include high-strength water hydraulic artificial muscles and robot arm joints.

PEIPEI LIU was born in Henan, China, in 1992. She received the M.A. degree in mechanical engineering from Dalian Maritime University, Dalian, in 2019. She is currently working in the field of mechanical structure design. Her research interests include product performance research and fluid dynamics research.

YONGJUN GONG was born in Shanxi, China, in 1974. He received the Ph.D. degree in mechanical and electronic control engineering from Zhejiang University, China, in 2005. He is currently a Professor and Doctoral Supervisor with the Naval Architecture and Ocean Engineering College, Dalian Maritime University, Dalian, China. He has published more than 50 articles in important academic journals and international conferences at home and abroad, of which more than 30 articles have been retrieved by the SCI and EI. His current research interests include water hydraulic control components and systems, underwater equipment development, ultra-high-pressure water jet rust removal and cutting technology, and wreck salvage technology.